



## A THREE-DIMENSIONAL DESCRIPTION OF SHAPE MEMORY ALLOY THERMOMECHANICAL BEHAVIOR INCLUDING PLASTICITY

**Sergio A. Oliveira, amserol@yahoo.com.br**

**Marcelo A. Savi, savi@mecanica.ufrj.br**

Universidade Federal do Rio de Janeiro  
COPPE – Departamento de Engenharia Mecânica  
Centro de Tecnologia – Sala G-204, Caixa Postal 68.503  
21.945.970 – Rio de Janeiro – RJ – Brasil

**Nestor Zouain, nestor@mecanica.ufrj.br**

Universidade Federal do Rio de Janeiro  
COPPE – Departamento de Engenharia Mecânica  
Centro de Tecnologia – Sala G-204, Caixa Postal 68.503  
21.945.970 – Rio de Janeiro – RJ – Brasil

*Abstract. This paper introduces a novel three-dimensional constitutive model that describes the thermomechanical behavior of shape memory alloys (SMAs). The model is developed within the framework of continuum mechanics and the standard generalized materials. Four macroscopic phases are considered associated with austenite and three variants of martensite, and each one of them can be induced either by volumetric or by deviatoric strains. The description of plasticity is also of concern in this constitutive model. Numerical simulations are carried out showing that the proposed model is able to capture the general thermomechanical behavior of SMAs for uniaxial and multiaxial tests.*

**Keywords:** *Shape Memory Alloy, constitutive model, plasticity.*

### 1. INTRODUCTION (TIMES NEW ROMAN, BOLD, SIZE 10)

Smart material systems and structures have a considerable importance nowadays being related to the design of adaptive systems that can mimic some aspects of natural systems. In general, it is possible to understand smart material properties as the coupling between different fields as mechanical, electrical, magnetic, temperature, among others. In the regard, several materials have been investigated and it is important to highlight shape memory alloys (SMAs), piezoelectric materials, magnetostrictive materials, electro-magneto rheological fluids.

SMAs have remarkable properties related to martensitic phase transformations. SMAs are usually employed in applications where large force or strains are required with low power consumption. A discussion about SMAs applications can be found in the following references: Lagoudas (2008), Paiva & Savi (2006), Machado & Savi (2003) and Kalamkarov & Kolpakov (1997).

The thermomechanical behavior of SMAs is very complex, presenting typical behaviors as pseudoelasticity, shape memory effect and phase transformation due to temperature variations, but also other interesting behaviors as the internal subloops due to the incomplete phase transformations, two-way shape memory effect, plasticity, transformation induced plasticity and rate dependence. All these phenomena justify the numerous research efforts related to the modeling and simulation of SMAs. The macroscopic constitutive modeling of SMAs relies on the continuum thermodynamics with internal state variables to take into account the changes in the microstructure due to phase transformation (Popov & Lagoudas, 2007; Paiva & Savi, 2006). Paiva & Savi (2006) and Lagoudas (2008) presented a general overview of the SMA modeling with the emphasis on the phenomenological constitutive models.

The three-dimensional description of the SMA thermomechanical behavior is even more complex. Besides the large number of complex phenomena involved, the lack of experimental data introduces more difficulties in the three-dimensional modeling. Among some research efforts dedicated to three-dimensional analysis of SMAs, it is important to highlight: Oliveira *et al.* (2010); Popov & Lagoudas (2007); Auricchio *et al.* (2007); Zaki & Moumni (2007); Panico & Brinson (2007); Levitas *et al.* (2003); Brocca *et al.* (2002); Souza *et al.* (1998); Fremond (1996). Besides, it is important to cite some experimental analysis related to multiaxial tests: Grabe & Bruhns (2007), McNaney *et al.* (2007), Manach & Favier (1997), Sittner *et al.* (1995), Wang *et al.* (2007), Auricchio (2007) and Panico & Brinson (2007).

Plastic behavior is an important issue related to SMA thermomechanical behavior. In general, it is possible to think in two different phenomena: classical plasticity and transformation induced plasticity (TRIP). A clear distinction can be established between both situations. Classical plasticity arises from applied stress or temperature variation, while TRIP is caused by phase proportions variation even for low constant stresses level, without reaching the yield surface of the weaker phase involved (Leblond *et al.*, 1989; Gautier *et al.*, 1989).

Plastic behavior in SMAs has been the objective of some research efforts. Baêta-Neves *et al.* (2004) and Paiva *et al.* (2005) presented the description of the plasticity in SMAs in one-dimensional media. The model considers the coupling

between the plasticity and the phase transformations. Recently, Hartl et al. (2010) explored the idea of the plastic behavior of the SMAs investigating the interaction between the phase transformations and the yield surface.

This article deals with the three-dimensional thermomechanical modeling of shape memory alloys including plasticity. The constitutive model is developed within the framework of the continuum mechanics and of the generalized standard materials. The model is inspired in the one-dimensional model that is able to describe different thermomechanical behaviors of SMAs in a flexible way, presenting numerical simulations that are in agreement with experimental uniaxial tests (Savi et al., 2002; Baêta Neves et al., 2004; Paiva et al., 2005; Savi & Paiva, 2005). Originally, this model is inspired on the Fremond's model (Fremond, 1996), implementing several modifications in order to match experimental data. The three-dimensional description using this model was previously addressed in Oliveira et al. (2010) that described the main features of the description here presented. Aguiar et al. (2010) employed this three-dimensional description to describe spring response, based on shear behavior. It is shown that this model is able to describe shear behavior, presenting good agreement with experimental tests. Here, a generalization of the three-dimensional model is presented, including plasticity and a new tensor to represent phase transformations. These modifications allow a proper description of thermomechanical behavior of SMA in three-dimensional media. A numerical procedure is proposed to deal with nonlinearities of the model and numerical simulations are carried out for uniaxial and multiaxial tests considering a homogeneous behavior of the SMA.

## 2. CONSTITUTIVE MODEL

The modeling of the thermomechanical behavior of SMAS can be done within the framework of the standard generalized materials, assuming that the thermodynamic state of the material is completely defined by a finite number of state variables (Lemaitre & Chaboche, 1990). Under this assumption, the thermomechanical behavior can be described by the Helmholtz free energy density,  $\psi$  and the pseudo-potential of dissipation  $\phi$ .

Experimental studies show that there are two possible phases in SMAS: austenite and martensite. In the martensitic phase, different strains orientations of crystallographic plates are considered what is known by martensitic variants. In the case of the three-dimensional, there are 24 possible variants martensitic. Concerning austenitic phase, only one variant exists (Zhang *et al.*, 1991, Schroeder & Wayman, 1977). The description of three-dimensional thermomechanical behavior of SMA is usually inspired in one-dimensional models and therefore, a limited number of martensitic variants are employed. Motivated by one-dimensional models, the proposed model considers four phases macroscopic: austenite ( $A$ ), the twinned martensite ( $M$ ), which is stable in the absence of a field of stress, and two other martensitic phases,  $M^+$  and  $M^-$ .

The definition of Helmholtz free energy density considers different expressions for each of the macroscopic phases, assuming that they are functions of the elastic strain  $\varepsilon_{ij}^e$ , temperature,  $T$ , isotropic hardening  $\vartheta$  and kinematic hardening  $\zeta_{ij}$ . The definition of these energy densities considers tensor quantities in principal axes.

$$\begin{aligned}
 M^+ : \rho\psi^+ (\varepsilon_{ij}^e, T, \vartheta, \zeta_{ij}) &= \frac{1}{2} (\lambda^M (\varepsilon_{kk}^e)^2 + 2\mu^M \varepsilon_{ij}^e \varepsilon_{ij}^e) - \alpha\Gamma - \Lambda^M - \Omega_{ij}^M (T - T_0) \varepsilon_{ij}^e + \frac{1}{2} K^M \vartheta^2 + \frac{1}{2HM} \zeta_{ij} \zeta_{ij} \\
 M^- : \rho\psi^- (\varepsilon_{ij}^e, T, \vartheta, \zeta_{ij}) &= \frac{1}{2} (\lambda^M (\varepsilon_{kk}^e)^2 + 2\mu^M \varepsilon_{ij}^e \varepsilon_{ij}^e) + \alpha\Gamma - \Lambda^M - \Omega_{ij}^M (T - T_0) \varepsilon_{ij}^e + \frac{1}{2} K^M \vartheta^2 + \frac{1}{2HM} \zeta_{ij} \zeta_{ij} \\
 A : \rho\psi^A (\varepsilon_{ij}^e, T, \vartheta, \zeta_{ij}) &= \frac{1}{2} (\lambda^A (\varepsilon_{kk}^e)^2 + 2\mu^A \varepsilon_{ij}^e \varepsilon_{ij}^e) - \Lambda^A - \Omega_{ij}^A (T - T_0) \varepsilon_{ij}^e \\
 &+ \frac{1}{2} K^A \vartheta^2 + \frac{1}{2HA} \zeta_{ij} \zeta_{ij} \\
 M : \rho\psi^M (\varepsilon_{ij}^e, T, \vartheta, \zeta_{ij}) &= \frac{1}{2} (\lambda^M (\varepsilon_{kk}^e)^2 + 2\mu^M \varepsilon_{ij}^e \varepsilon_{ij}^e) + \Lambda^M - \Omega_{ij}^M (T - T_0) \varepsilon_{ij}^e + \frac{1}{2} K^M \vartheta^2 + \frac{1}{2HM} \zeta_{ij} \zeta_{ij}
 \end{aligned} \tag{1}$$

In the previous equations, subscript  $A$  and  $M$  are related to austenite phases and martensite, respectively;  $\lambda$  and  $\mu$  are the Lamé coefficients;  $\alpha$  is a parameter that control the size of hysteresis loop;  $\Lambda^M$  and  $\Lambda^A$  are functions of temperature that define the phase transformation stress;  $\Omega_{ij}$  is a tensor related to the thermal expansion coefficients,  $T_0$  is a reference temperature in a stress-free state,  $K$  it is the plastic modulus,  $H$  is the kinematical hardening modulus;  $\vartheta$  is related to isotropic hardening and  $\zeta_{ij}$  is kinematic hardening tensor; finally,  $\rho$  is the material density.

An equivalent strain field,  $\Gamma$ , governs phase transformations being defined as follows:

$$\Gamma = \frac{1}{3} \varepsilon_{kk}^e + \frac{2}{3} \sqrt{J_2^e} |\text{sign}(\varepsilon_{kk}^e)| \tag{2}$$

Note that this strain field has volumetric and deviatoric terms that are respectively given by:

$$\varepsilon_{kk}^e = \varepsilon_{11}^e + \varepsilon_{22}^e + \varepsilon_{33}^e \tag{3}$$

$$J_2^e = \frac{1}{6} \{ (\varepsilon_{11}^e - \varepsilon_{22}^e)^2 + (\varepsilon_{22}^e - \varepsilon_{33}^e)^2 + (\varepsilon_{33}^e - \varepsilon_{11}^e)^2 + 6((\varepsilon_{12}^e)^2 + (\varepsilon_{13}^e)^2 + (\varepsilon_{23}^e)^2) \} \tag{4}$$

$$\text{where } \text{sign}(\varepsilon_{kk}^e) = \begin{cases} +1, & \text{if } \varepsilon_{kk}^e \geq 0 \\ -1, & \text{if } \varepsilon_{kk}^e < 0 \end{cases} \quad (5)$$

It should be highlighted again that this equivalent strain field  $\Gamma$  can be induced either by volumetric expansion (represented by the first term of the Equation 2) or deviatoric expansion. This hypothesis is based on experimental observations that show that both effects induce the phase transformations. It is important to point out that shear experimental tests indicate that the curves of stress-strain are qualitatively similar to the curves in the tensile tests (Jackson et al., 1972; Manach & Favier, 1997; Aguiar et al., 2010). Under this assumption, the equivalent field  $\Gamma$  may be interpreted as a phase transformation inductor that defines what kind of martensitic variant is induced. Besides, note that for one-dimensional case,  $\varepsilon_{11}^e$ , reducing the model to the original one-dimensional description variant can be induced either by volumetric or by shear effects, allowing a proper description of the three-dimensional behavior (Savi et al., 2002; Paiva et al., 2005; Aguiar et al., 2010). Moreover, it should be pointed out that, since the sign of shear strains does not appear in this inductor, they have a neutral influence, tending to follow the volumetric expansion.

At this moment, it is necessary to define the free energy density of the mixture, setting the volume fraction of martensite variants  $\beta^+$  and  $\beta^-$ , associated with detwinned martensite ( $M^+$  and  $M^-$ , respectively) and  $\beta^A$ , for the austenite ( $A$ ). The fourth phase is associated with twinned martensite ( $M$ ) and its volume fraction is  $\beta^M$ .

$$\rho\psi(\varepsilon_{ij}^e, T, \vartheta, \varsigma_{ij}, \beta^+, \beta^-, \beta^A, \beta^M) = \rho \sum_{n=1}^4 \beta^n \psi^n(\varepsilon_{ij}^e, T, \vartheta, \varsigma_{ij}) + I_\theta(\beta^+, \beta^-, \beta^A, \beta^M) \quad (6)$$

where  $I_\theta(\beta^+, \beta^-, \beta^A, \beta^M)$  is the indicator function associated with the convex set  $\theta$  (Rockafellar, 1970) establishing the conditions for phase's coexistence:

$$\theta = \{\beta^n \in \mathfrak{R} | 0 \leq \beta^n \leq 1 (n = +, -, A, M); \beta^+ + \beta^- + \beta^A + \beta^M = 1\} \quad (7)$$

Besides the restrictions related to the phase's coexistence, there are extra constraints that avoids that phases  $M^+$  and  $M^-$  are induced in a stress free state. Furthermore, phases  $M^+$  and  $M^-$  should not appear together. The existence of a phase is defined by the signal of the inductor,  $\Gamma$ , and the values of  $\beta^+, \beta^-, \beta^A, \beta^M$ .

Based on these conditions, it is possible to use  $\beta^M = 1 - \beta^+ - \beta^- - \beta^A$  in order to define the free energy density in terms of three volume fractions:

$$\rho\psi(\varepsilon_{ij}^e, T, \vartheta, \varsigma_{ij}, \beta^+, \beta^-, \beta^A) = \rho\{\beta^+(\psi^+ - \psi^M) + \beta^-(\psi^- - \psi^M) + \beta^A(\psi^A - \psi^M) + \psi^M\} + I_\pi(\beta^+, \beta^-, \beta^A) \quad (8)$$

Now, the indicator function  $I_\pi(\beta^+, \beta^-, \beta^A)$  is related to the convex set defined as follows, which can be geometrically interpreted by a tetrahedron in  $\beta^+, \beta^-, \beta^A$ -space, shown in Figure 1.

$$\pi = \{\beta^n \in \mathfrak{R} | 0 \leq \beta^n \leq 1 (n = +, -, A); \beta^+ + \beta^- + \beta^A = 1\} \quad (9)$$

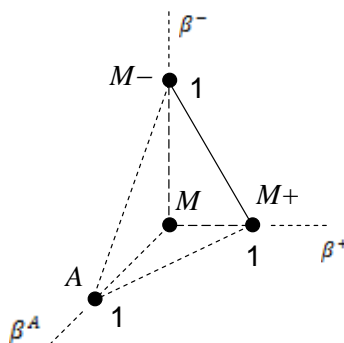


Figure 1 – Geometrical representation of the phase's coexistence restriction.

Under these assumptions, the free energy density of the mixture has the following form:

Sergio A. Oliveira, Marcelo A.Savi, Nestor Zouain

### A Three-dimensional Description of Shape Memory Alloy Thermomechanical Behavior Including Plasticity

$$\rho\psi(\varepsilon_{ij}^e, T, \vartheta, \varsigma_{ij}, \beta^+, \beta^-, \beta^A) = \alpha\Gamma(\beta^- - \beta^+) - \Lambda(\beta^+ + \beta^-) + \left\{\frac{1}{2}(\lambda^A - \lambda^M)(\varepsilon_{kk}^e)^2 + (\mu^A - \mu^M)\varepsilon_{ij}^e\varepsilon_{ij}^e - (\Omega_{ij}^A - \Omega_{ij}^M)(T - T_0)\varepsilon_{ij}^e - \Lambda^N + \frac{1}{2}(K^A - K^M)\vartheta^2 + \left(\frac{1}{2HA} - \frac{1}{2HM}\right)\varsigma_{ij}\varsigma_{ij}\right\}\beta^A + \left\{\frac{1}{2}\lambda^M(\varepsilon_{kk}^e)^2 + \mu^M\varepsilon_{ij}^e\varepsilon_{ij}^e\right\} - \Omega_{ij}^M(T - T_0)\varepsilon_{ij}^e + \Lambda^M + \frac{1}{2}K^M\vartheta^2 + \frac{1}{2HM}\varsigma_{ij}\varsigma_{ij} + I_\pi(\beta^+, \beta^-, \beta^A) \quad (10)$$

where  $\Lambda = 2\Lambda^M$  and  $\Lambda^N = \Lambda^M + \Lambda^A$ .

Now, an additive decomposition is assumed by considering that the total strain,  $\varepsilon_{ij}$ , is the sum of the elastic strain  $\varepsilon_{ij}^e$ , the plastic strain,  $\varepsilon_{ij}^p$  and the phase transformation,  $\varepsilon_{ij}^{phase}$ :

$$\varepsilon_{ij}^e = \varepsilon_{ij} - \varepsilon_{ij}^p + \varepsilon_{ij}^{phase} \quad (11)$$

The phase transformation strain establishes the control of the horizontal size of the stress-strain hysteresis loop, being defined as follows:

$$\varepsilon_{ij}^{phase} = \alpha_{ijkl}^h r_{kl}(\beta^- - \beta^+) \quad (12)$$

where  $\alpha_{ijkl}^h$  is a fourth-order tensor related to phase transformations that considers different parameters for normal and shear behaviors, as represented below.

$$\alpha_{ijkl}^h = \begin{bmatrix} \alpha_N^h & \alpha_N^h - \alpha_S^h & \alpha_N^h - \alpha_S^h & 0 & 0 & 0 \\ \alpha_N^h - \alpha_S^h & \alpha_N^h & \alpha_N^h - \alpha_S^h & 0 & 0 & 0 \\ \alpha_N^h - \alpha_S^h & \alpha_N^h - \alpha_S^h & \alpha_N^h & 0 & 0 & 0 \\ 0 & 0 & 0 & \alpha_S^h & 0 & 0 \\ 0 & 0 & 0 & 0 & \alpha_S^h & 0 \\ 0 & 0 & 0 & 0 & 0 & \alpha_S^h \end{bmatrix} \quad (13)$$

$r_{kl}$  is a second-order tensor defined as follows:

$$r_{kl} = \frac{S_{kl}^{max}}{|S_{kl}^{max}|} \quad (14)$$

where  $S_{kl}^{max}$  represents the maximum value of the mechanical loading that can be a stress or a strain. Note that this value is calculated by assuming the maximum value of  $\frac{S_{kl}^{max}}{|S_{kl}^{max}|} = 0$  if  $S_{kl}^{max} = 0$ . Therefore, we can write:

$$r_{kl} = \begin{cases} +1, & \text{if } S_{kl}^{max} > 0 \\ 0 & S_{kl}^{max} = 0 \\ -1, & \text{if } S_{kl}^{max} < 0 \end{cases} \quad (15)$$

From the generalized standard materials approach, the thermodynamical forces associated with each internal variable are defined as follows (Lemaitre & Chaboche, 1990):

$$\sigma_{ij} = \rho \frac{\partial \psi}{\partial \varepsilon_{ij}^e} = \lambda \varepsilon_{kk}^e \delta_{ij} + 2\mu \varepsilon_{ij}^e + \alpha \omega_{ij}(\beta^- - \beta^+) - \Omega_{ij}(T - T_0) \quad (16)$$

$$B^+ \in -\rho \partial_{\beta^+}(\psi) = \Gamma\alpha + \Lambda + P^+ - \alpha_{ijkl}^h r_{kl} \Omega_{ij}(T - T_0) - \tau^+ \quad (17)$$

$$B^- \in -\rho \partial_{\beta^-}(\psi) = -\Gamma\alpha + \Lambda - P^- + \alpha_{ijkl}^h r_{kl} \Omega_{ij}(T - T_0) - \tau^- \quad (18)$$

$$B^A \in -\rho \partial_{\beta^A}(\psi) = \Lambda^N + P^A + \varepsilon_{ij}^e(\Omega_{ij}^A - \Omega_{ij}^M)(T - T_0) - \frac{1}{2}(K^A - K^M)\vartheta^2 - \left(\frac{1}{2HA} - \frac{1}{2HM}\right)\varsigma_{ij}\varsigma_{ij} - \tau^A \quad (19)$$

$$X_{ij} = -\rho \frac{\partial \psi}{\partial \varepsilon_{ij}^p} = \lambda \varepsilon_{kk}^e \delta_{ij} + 2\mu \varepsilon_{ij}^e + \alpha \omega_{ij}(\beta^- - \beta^+) - \Omega_{ij}(T - T_0) = \sigma_{ij} \quad (20)$$

$$Y \in -\rho \frac{\partial \psi}{\partial \vartheta} = -K \vartheta \quad (21)$$

$$Z_{ij} \in -\rho \frac{\partial \psi}{\partial \varsigma_{ij}} = -\frac{1}{H} \varsigma_{ij} \quad (22)$$

where  $B^i, R_{ij}, X_{ij}, Y$  e  $Z_{ij}$  represents the thermodynamics forces,  $\sigma_{ij}$  represents the stress tensor and, associated with the three volumetric fractions respectively,  $\tau(\beta^+, \beta^-, \beta^A)$  is the sub-differential with respect to the Geometrical representation of the phase's coexistence restriction, Fig.1 such as:

$$\tau = (\tau^+, \tau^-, \tau^A) \in \partial I_\pi(\beta^+, \beta^-, \beta^A) \quad (23)$$

And  $P^+, P^-, P^A$ , and are auxiliary variables given by:

$$P^+ = (\lambda \varepsilon_{kk}^e \alpha_{ijkl}^h r_{kl} \delta_{ij} + 2\varepsilon_{ij}^e \alpha_{ijkl}^h r_{kl} \mu) + \alpha(\beta^- - \beta^+) \left\{ \frac{1}{3} \alpha_{ijkl}^h r_{kl} \delta_{ij} + \frac{2J^\alpha}{\sqrt{|3J_2^e|}} \text{sign}(\varepsilon_{kk}^e) \right\} \quad (24)$$

$$P^- = -(\lambda \varepsilon_{kk}^e \alpha_{ijkl}^h r_{kl} \delta_{ij} + 2\varepsilon_{ij}^e \alpha_{ijkl}^h r_{kl} \mu) - \alpha(\beta^- - \beta^+) \left\{ \frac{1}{3} \alpha_{ijkl}^h r_{kl} \delta_{ij} + \frac{2J^\alpha}{\sqrt{|3J_2^e|}} \text{sign}(\varepsilon_{kk}^e) \right\} \quad (25)$$

$$P^A = -\frac{1}{2} (\lambda^A (\varepsilon_{kk}^e)^2 + 2\mu^A \varepsilon_{ij}^e \varepsilon_{ij}^e) + \frac{1}{2} (\lambda^M (\varepsilon_{kk}^e)^2 + 2\mu^M \varepsilon_{ij}^e \varepsilon_{ij}^e) \quad (26)$$

Moreover, it is defined

$$J^\alpha = \frac{\alpha_S^h}{6} \{ (r_{11} - r_{22})(\varepsilon_{11}^e - \varepsilon_{22}^e) + (r_{22} - r_{33})(\varepsilon_{22}^e - \varepsilon_{33}^e) + (r_{33} - r_{11})(\varepsilon_{33}^e - \varepsilon_{11}^e) \} \quad (27)$$

Note that material parameters can be defined by considering a kind of rule of mixtures as follows:

$$\begin{aligned} \lambda &= \lambda^M + \beta^A (\lambda^A - \lambda^M) \\ \mu &= \mu^M + \beta^A (\mu^A - \mu^M) \\ \Omega_{ij} &= \Omega_{ij}^M + \beta^A (\Omega_{ij}^A - \Omega_{ij}^M) \\ K &= K^M + \beta^A (K^A - K^M) \\ \frac{1}{H} &= \frac{1}{H^M} + \beta^A \left( \frac{1}{H^A} - \frac{1}{H^M} \right) \end{aligned} \quad (28)$$

It is also important to observe that:

$$\omega_{ij} = \frac{1}{3} \delta_{ij} + \left[ \frac{3\varepsilon_{ij}^e - \varepsilon_{kk}^e \delta_{ij}}{3\sqrt{|3J_2^e|}} \right] \text{sign}(\varepsilon_{kk}^e) \quad (29)$$

And, since  $\lambda \varepsilon_{kk}^e \delta_{ij} + 2\mu \varepsilon_{ij}^e = E_{ijkl} \varepsilon_{kl}^e$ , it is possible to rewrite the stress-strain relation as follows:

$$\sigma_{ij} = E_{ijkl} \varepsilon_{kl}^e + \alpha \omega_{ij} (\beta^- - \beta^+) - \Omega_{ij} (T - T_0) \quad (30)$$

where  $E_{ijkl} = E_{ijkl}^M + \beta^A (E_{ijkl}^A - E_{ijkl}^M)$  refers to the elastic modulus tensor. In case of isotropic materials, the coefficients of Lamé can be expressed in terms of the engineering constants as follows:

$$\lambda = \frac{\nu E}{(1+\nu)(1-2\nu)} \quad \text{and} \quad G = \frac{E}{2(1+\nu)} \quad (31)$$

where  $E$  is the elastic modulus,  $G$  is the shear modulus and  $\nu$  is the Poisson's coefficient.

The functions  $\Lambda$  and  $\Lambda^N$  are temperatures dependent being defined as follows:

$$\Lambda = 2 \Lambda^M = \begin{cases} -L_0^\pm + \frac{L^\pm}{T_M} (T - T^M) & \text{if } T > T^M \\ -L_0^\pm & \text{if } T \leq T^M \end{cases} \quad (32)$$

Sergio A. Oliveira, Marcelo A.Savi, Nestor Zouain  
A Three-dimensional Description of Shape Memory Alloy Thermomechanical Behavior Including Plasticity

$$\Lambda^s = \Lambda^M + \Lambda^A = \begin{cases} -L_0^A + \frac{L^A}{T^M}(T - T^M) & \text{if } T > T^M \\ -L_0^A & \text{if } T \leq T^M \end{cases} \quad (33)$$

where  $T^M$  is the temperature below which the martensitic phase becomes stable. Besides,  $L_0^\pm$ ,  $L^\pm$ ,  $L_0^A$  and  $L^A$  are parameters related to phase transformation critical stresses. Note that, based on the previous definition, the phase transformation stress level is constant for  $T < T^M$ .

The thermomechanical behavior of SMAs is intrinsically dissipative and therefore, it is important to establish the pseudo-potential of dissipation that allows the description of dissipative materials. By assuming that this potential may be split into mechanical,  $\Phi^{Mech}$ , and thermal,  $\Phi^{Heat}$ , parts, its mechanical part may be considered as follows:

$$\Phi = \Phi(\varepsilon_{ij}^e, \varepsilon_{ij}^{tp}, \varepsilon_{ij}^p, \vartheta, \zeta_{ij}, \beta^n, q) = \Phi^{Mech}(\varepsilon_{ij}^e, \varepsilon_{ij}^{tp}, \varepsilon_{ij}^p, \vartheta, \zeta_{ij}, \beta^n) + \Phi^{Heat}(q) \quad (34)$$

where  $\Phi^{Mech}$  is the mechanical part and  $\Phi^{Heat}$  is the thermal part.

Using the dual of the pseudo-potential of dissipation, its mechanical part can be expressed by the following equation:

$$\overline{\Phi}^{Mech}(B^+, B^-, B^A, X_{ij}, Y, Z_{ij}) = \frac{1}{2\eta^+}(B^+ + \eta^l Y + \eta_{ij}^K Z_{ij})^2 + \frac{1}{2\eta^-}(B^- + \eta^l Y + \eta_{ij}^K Z_{ij})^2 + \frac{1}{2\eta^A}(B^A - \eta^l Y - \eta_{ij}^K Z_{ij})^2 + I_{\bar{\chi}}(B^+, B^-, B^A) + I_f(X_{ij}, Y, Z_{ij}) \quad (35)$$

By considering again the generalized standard materials approach, the thermodynamical fluxes are represented as (Lemaitre & Chaboche, 1990):

$$\dot{\beta}^+ \in \partial_{B^+}(\overline{\Phi}^{Mech}) = \frac{B^+}{\eta^+} + \frac{\eta^l}{\eta^+} Y + \frac{\eta_{ij}^K}{\eta^+} Z_{ij} + \partial_{B^+} I_{\bar{\chi}} = \frac{B^+}{\eta^+} + \frac{\eta^l}{\eta^+} \vartheta + \frac{\eta_{ij}^K \zeta_{ij}}{\eta^+ H} + \gamma^+ \quad (36)$$

$$\dot{\beta}^- \in \partial_{B^-}(\overline{\Phi}^{Mech}) = \frac{B^-}{\eta^-} + \frac{\eta^l}{\eta^-} Y + \frac{\eta_{ij}^K}{\eta^-} Z_{ij} + \partial_{B^-} (I_{\bar{\chi}}) = \frac{B^-}{\eta^-} + \frac{\eta^l}{\eta^-} \vartheta + \frac{\eta_{ij}^K \zeta_{ij}}{\eta^- H} + \gamma^- \quad (37)$$

$$\dot{\beta}^A \in \partial_{B^A}(\overline{\Phi}^{Mech}) = \frac{B^A}{\eta^A} + \frac{\eta^l}{\eta^A} Y + \frac{\eta_{ij}^K}{\eta^A} Z_{ij} + \partial_{B^A} (I_{\bar{\chi}}) = \frac{B^A}{\eta^A} + \frac{\eta^l}{\eta^A} \vartheta + \frac{\eta_{ij}^K \zeta_{ij}}{\eta^A H} + \gamma^A \quad (38)$$

$$\dot{\varepsilon}_{ij}^p \in \partial_{X_{ij}}(\overline{\Phi}^{Mech}) = \gamma \text{sign}(d_{ij} - \zeta_{ij}) \quad (39)$$

$$\dot{\vartheta} \in \partial_Y(\overline{\Phi}^{Mech}) = \sqrt{\frac{2}{3}} \gamma + \eta^l (\dot{\beta}^+ + \dot{\beta}^- + \dot{\beta}^A) = \sqrt{\frac{2}{3}} |\varepsilon_{ij}^p| + \eta^l (\dot{\beta}^+ + \dot{\beta}^- + \dot{\beta}^A) \quad (40)$$

$$\begin{aligned} \dot{\zeta}_{ij} \in \partial_{Z_{ij}}(\overline{\Phi}^{Mech}) &= \frac{2}{3} \gamma H \text{sign}(d_{ij} - \zeta_{ij}) + \eta_{ij}^K (\dot{\beta}^+ + \dot{\beta}^- + \dot{\beta}^A) \\ &= \frac{2}{3} H \dot{\varepsilon}_{ij}^p + \eta_{ij}^K (\dot{\beta}^+ + \dot{\beta}^- + \dot{\beta}^A) \end{aligned} \quad (41)$$

where  $\eta^m$  ( $m = +, -, A$ ) is associated with the internal dissipation of each material phase, while  $\eta^l$  and  $\eta_{ij}^K$  are parameters of the coupling between phase transformations and plasticity respectively associated with the isotropic and kinematic hardening;  $\gamma(\dot{\beta}^+, \dot{\beta}^-, \dot{\beta}^A)$  is the sub-differential with respect to the convex set the  $\chi$  conforme, defined conform the Equations 48 e 49, shown conform Equation 42.

$$\gamma = (\gamma^+, \gamma^-, \gamma^A) \in \partial I_{\bar{\chi}}(\dot{\beta}^+, \dot{\beta}^-, \dot{\beta}^A) \quad (42)$$

$\gamma$  is the plastic multiplier and  $d_{ij}$  is the deviatoric tensor of  $\sigma_{ij}$ , defined as

$$d_{ij} = \sigma_{ij} - \frac{1}{3} \sigma_{kk} \delta_{ij} \quad (43)$$

$I_f$  is the indicator function related to the classic plasticity;  $f$  is defined from the characteristics of the yield surface as follows (Simo & Hughes, 1998).

$$f = |d_{ij} - \zeta_{ij}| - \sqrt{\frac{2}{3}} (\sigma_Y - K\vartheta) \quad (44)$$

subjected to the Kuhn-Tucker conditions presented as follows:

$$\gamma \geq 0, \quad f(\sigma_{ij}, \varsigma_{ij}, \vartheta) \leq 0 \quad \text{and} \quad \gamma f(\sigma_{ij}, \varsigma_{ij}, \vartheta) = 0 \quad (45)$$

and the consistency conditions:

$$\dot{\gamma} f(\sigma_{ij}, \varsigma_{ij}, \vartheta) = 0 \quad (46)$$

The yield surface is defined by  $\sigma_Y$  that has different values for the austenitic and martensitic phases. Their values are temperature dependent tending to decrease for high temperatures. Different expressions can be employed for the proper description of these conditions. Here, for the sake of simplicity, temperature variation is assumed as:

$$\begin{cases} \sigma_Y = \sigma_Y^M \text{ if } T \leq T^M \\ \sigma_Y = \frac{\sigma_Y^M(T^A - T) + \sigma_Y^{A,i}(T - T^M)}{T^A - T^M} \text{ if } T^M < T \leq T^A \\ \sigma_Y = \frac{\sigma_Y^{A,i}(T^F - T) + \sigma_Y^F(T - T^A)}{T^F - T^A} \text{ if } T^M < T \leq T^F \end{cases} \quad (47)$$

where  $T^F$  is the temperature of reference for determination of the yield stress for high temperatures, and  $T^A$  is the temperature above of the austenitic phase is stable;  $T^M$  is the temperature below of the martensitic phase is stable;  $\sigma_Y^{A,i}$  and  $\sigma_Y^{A,f}$  defines the thermal variation of the yield stress of the austenitic phase.

The term  $I_\chi$  is an indicator function of the convex set  $\chi$  that defines restrictions associated with the phase evolution. Physically, this function considers the restrictions for the internal sub-loops due to incomplete phase transformations and also avoids improper phase transformations (Savi & Paiva 2005).

Therefore, for  $\sigma_{ij} \neq 0$ , the convex set  $\chi$  can be written as follows:

$$\chi = \left\{ \dot{\beta}^n \in \mathfrak{R} \left| \begin{array}{l} \dot{\Gamma} \dot{\beta}^+ \geq 0; \dot{\Gamma} \dot{\beta}^A \leq 0 \text{ if } \dot{\Gamma} > 0 \\ \dot{\Gamma} \dot{\beta}^- \leq 0; \dot{\Gamma} \dot{\beta}^A \geq 0 \text{ if } \dot{\Gamma} < 0 \end{array} \right. \right\} \quad (48)$$

and for  $\sigma_{ij} = 0$ :

$$\chi = \left\{ \dot{\beta}^n \in \mathfrak{R} \left| \begin{array}{l} \left\{ \begin{array}{l} \dot{T} \dot{\beta}^+ < 0 \text{ if } \dot{T} > 0, \beta_s^+ \neq 0 \\ \dot{T} \dot{\beta}^+ = 0, \text{ otherwise} \end{array} \right. \\ \left\{ \begin{array}{l} \dot{T} \dot{\beta}^- < 0 \text{ if } \dot{T} > 0, \beta_s^- \neq 0 \\ \dot{T} \dot{\beta}^- = 0, \text{ otherwise} \end{array} \right. \\ \dot{T} \dot{\beta}^A \geq 0 \\ -(\dot{\beta}^+)^2 - \dot{\beta}^+ \dot{\beta}^A = 0 \\ -(\dot{\beta}^-)^2 - \dot{\beta}^- \dot{\beta}^A = 0 \end{array} \right. \right\} \quad (49)$$

This set also expresses restrictions to improper phase transformations of  $M^+ \rightarrow M$  and  $M^- \rightarrow M$ , expressed respectively, by:

$$\begin{cases} \dot{\beta}^+ \dot{\beta}^M = \dot{\beta}^+ (-\dot{\beta}^+ - \dot{\beta}^- - \dot{\beta}^A) = -(\dot{\beta}^+)^2 - \dot{\beta}^+ \dot{\beta}^A = 0 \\ \dot{\beta}^- \dot{\beta}^M = \dot{\beta}^- (-\dot{\beta}^+ - \dot{\beta}^- - \dot{\beta}^A) = -(\dot{\beta}^-)^2 - \dot{\beta}^- \dot{\beta}^A = 0 \end{cases} \quad (50)$$

In order to contemplate the different characteristics for the kinetic of the phase transformation in the loading and unloading processes, different values are employed for the parameters  $\eta^m$  ( $m = +, -, A$ ), in the follow form:

$$\begin{cases} \eta^m = \eta_L^m \text{ if } \dot{\Gamma} > 0 \\ \eta^m = \eta_U^m \text{ if } \dot{\Gamma} < 0 \end{cases} \quad (51)$$

At this moment, there is a complete set of constitutive equations that describes the SMA thermomechanical behavior, summarized by the following set of equations:

Sergio A. Oliveira, Marcelo A.Savi, Nestor Zouain

A Three-dimensional Description of Shape Memory Alloy Thermomechanical Behavior Including Plasticity

$$\sigma_{ij} = E_{ijkl}\varepsilon_{kl}^e + \alpha\omega_{ij}(\beta^- - \beta^+) - \Omega_{ij}(T - T_0) \quad (52)$$

$$\dot{\beta}^+ = \frac{1}{\eta^+} \left\{ \Gamma\alpha + \Lambda + P^+ - \alpha_{ijkl}^h r_{kl} \Omega_{ij}(T - T_0) - \eta^l K \vartheta - \eta_{ij}^K \frac{s_{ij}}{H} - \tau^+ \right\} + \gamma^+ \quad (53)$$

$$\dot{\beta}^- = \frac{1}{\eta^-} \left\{ -\Gamma\alpha + \Lambda - P^- + \alpha_{ijkl}^h r_{kl} \Omega_{ij}(T - T_0) - \eta^l K \vartheta - \eta_{ij}^K \frac{s_{ij}}{H} - \tau^- \right\} + \gamma^- \quad (54)$$

$$\begin{aligned} \dot{\beta}^A = \frac{1}{\eta^A} \left\{ P^A + \Lambda^{\kappa} + \bar{\varepsilon}_{ij}^e (\Omega_{ij}^A - \Omega_{ij}^M)(T - T_0) - \frac{1}{2}(K^A - K^M)\vartheta^2 - \left( \frac{1}{2H^A} - \frac{1}{2H^M} \right) s_{ij}s_{ij} + \right. \\ \left. \eta^l K \vartheta + \eta_{ij}^K \frac{s_{ij}}{H} - \tau^A \right\} + \gamma^A \end{aligned} \quad (55)$$

$$\varepsilon_{ij}^p = \gamma \text{sign}(d_{ij} - s_{ij}) \quad (56)$$

$$\dot{\vartheta} = \sqrt{\frac{2}{3}} \gamma + \eta^l (\dot{\beta}^+ + \dot{\beta}^- + \dot{\beta}^A) \quad (57)$$

$$\dot{s}_{ij} = \frac{2}{3} H \varepsilon_{ij}^p + \eta_{ij}^K (\dot{\beta}^+ + \dot{\beta}^- + \dot{\beta}^A) \quad (58)$$

At this point, it is important to recall some aspects of phase transformations. On the one hand, if  $\Gamma \geq 0$  the variant  $M^+$  is induced, increasing the value of  $\beta^+$  ( $\Gamma \geq 0 \rightarrow M^+$ ). On the other hand, the variant  $M^-$  is induced when  $\Gamma < 0$  ( $\Gamma < 0 \rightarrow M^-$ ), increasing the value of  $\beta^-$ . Moreover, it should be pointed out that, since the sign of shear strains does not appear in this inductor, they have a neutral influence, tending to follow the volumetric expansion.

In order to deal with the nonlinearities of the formularization, the solution of the constitutive equations employs the operator split technique (Ortiz et al., 1983) associated to an iterative procedure. Under this assumption, the coupled equation is solved as sets of uncoupled problems. In this section, first, the numerical procedure for the phase transformation is presented and immediately afterwards the referring procedure to the plasticity.

Phase transformation problem is treated by assuming the operator split technique. The predictor step assumes that phase transformation does not occur, defining a trial state where volume fractions are identical to the previous state. Mathematically speaking, this procedure implies to neglect the sub-differentials. Therefore, the Euler implicit method is employed to calculate the volume fractions ( $\beta^+, \beta^-, \beta^A$ ). If the trial state obeys the restrictions represented for the tetrahedron of Figure 2, then it is the actual state. Otherwise, the sub-differentials needs to be calculated by orthogonal projections to the boundary of the domain represented tetrahedron of Figure 2. This projection is based on the nearest point on the surface of the tetrahedron of Figure 2, and is calculated step by step, according to the restrictions imposed by the indicatriz function  $I_\pi$ . At each step the sub-differentials is calculated decreasing the distance between the surface of the tetrahedron and the point that defines the values of the volumetric fractions considered until this distance is equal to zero. This projection assures that the calculated volume fractions obey the internal restrictions imposed by the model (Savi & Braga, 1993). An iterative numerical procedure assures that this approach converges.

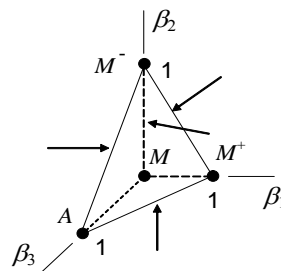


Figure 2 – Projection algorithm for phase transformation.

The elasto-plastic numerical approach considers the classical return-mapping algorithm (Simo & Hughes, 1998). The general idea is similar to the one employed for phase transformation problem. Initially, it is assumed a trial state where plastic strains do not occur. Then, constraints related to yield surface are analyzed. Return mapping algorithm is employed to perform the projection from the trial to actual state.

The plastic flow is governed by the following equations:

$$\varepsilon_{ij}^p = \gamma \varphi_{ij} \quad (59)$$

$$\dot{\zeta}_{ij} = \gamma \frac{2}{3} H \varphi_{ij} \quad (60)$$

$$\dot{\vartheta} = \gamma \sqrt{\frac{2}{3}} \quad (61)$$

where  $\varphi_{ij}$  is the normal unit vector of the Von Mises yield surface, defined as follows

$$\varphi_{ij} = \frac{d_{ij} - s_{ij}}{|\zeta_{ij}|} = \frac{\zeta_{ij}}{|\zeta_{ij}|} = \frac{\partial f(\sigma_{ij}, s_{ij})}{\partial \sigma_{ij}} \quad (62)$$

where  $\zeta_{ij} = d_{ij} - s_{ij}$ .

The implicit Euler method is employed to discretize the equations. The trial state is defined by assuming that no plastic strain occur:

$$(f^{trial})_{n+1} = \left| (\zeta_{ij}^{trial})_{n+1} \right| - \sqrt{\frac{2}{3}} (\sigma^Y - K \vartheta_n) \quad (63)$$

If the trial state is admissible:

$$(f^{trial})_{n+1} \leq 0 \quad (64)$$

Under this condition, the actual state is the actual one. Otherwise, the trial state is not admissible,  $(f^{trial})_{n+1} > 0$ , and the Kuhn-Tucker conditions are violated. Therefore, it is necessary to calculate the actual state using the return mapping algorithm. This is the correction step, performed using the plastic multiplier,  $\Delta\gamma$ , that establishes the projection in the yield surface where  $f_{n+1} = 0$ . Figure 3 presents the projection from the trial to the actual state.

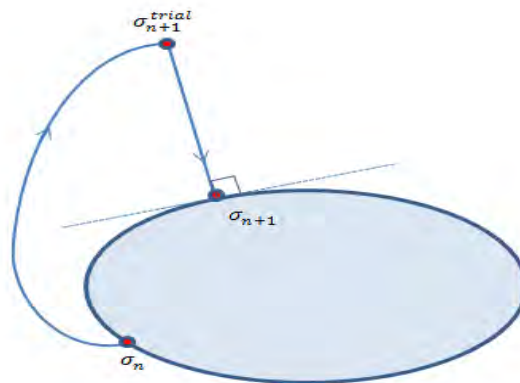


Figure 3 - Return-mapping algorithm.

The plastic multiplier is defined by the following expression:

$$\gamma_{n+1} = \frac{f_{n+1}^{trial}}{2\mu + \frac{2}{3}(H+K)} \frac{1}{\Delta t} \quad (65)$$

### 3. NUMERICAL SIMULATIONS – UNIAXIAL TESTS

The objective of this section is to evaluate the capability of the proposed model to describe the thermomechanical behavior of SMAs in one-dimensional media. Typical behaviors are treated, including pseudoelasticity and shape memory effect. Table 1 presents the parameters employed for the numerical simulations. These parameters are based on experimental results due to Tobushi et al. (1991) that considers pseudoelastic tests at three different temperatures. Poisson ratio vanishes for the one-dimensional tests.

Sergio A. Oliveira, Marcelo A.Savi, Nestor Zouain

A Three-dimensional Description of Shape Memory Alloy Thermomechanical Behavior Including Plasticity

Table 1 - Model parameters based on experimental tests due to Tobushi et al. (1991).

$E^A$ (GPa)	$E^M$ (GPa)	$\Omega^A$ (MPa/K)	$\Omega^M$ (MPa/K)	$\alpha_N^h$ (MPa)	$\alpha_S^h$ (MPa)	$\alpha$ (MPa)
54	42	0.74	0.17	0.0473	0.02	330
$L_0^+$ (MPa)	$L^+$ (MPa)	$L_0^A$ (MPa)	$L^A$ (MPa)	$T^M$ (K)	$T_0$ (K)	$T^A$ (K)
0.15	41.5	0.63	185	291.4	307	307.5
$T^{A,f}$ (K)	$\sigma_Y^M$ (GPa)	$\sigma_Y^{A,i}$ (GPa)	$\sigma_Y^{A,f}$ (GPa)	$K^A$ (GPa)	$K^M$ (GPa)	$H^A$ (GPa)
423	0.5	1.5	1	1.4	0.4	4
$H^M$ (GPa)	$\eta^I$	$\eta^K$	$\eta_L^+$ (MPa.s)	$\eta_U^-$ (MPa.s)	$\eta_L^-$ (MPa.s)	$\eta_U^-$ (MPa.s)
1.1	-0.01	-0.01	1	2.7	1	2.7
$\eta_U^A$ (MPa.s)	$\eta_U^A$ (MPa.s)					
1	2.7					

Numerical simulations are now performed for pseudoelastic tests trying to match experimental data of Tobushi et al. (1991), performed at three different temperatures:  $T = 373$  K,  $T = 353$  K and  $T = 333$  K. Figure 4 presents these results establishing a comparison between numerical and experimental data, showing a good agreement. Note that results capture the general behavior that includes the hysteresis loop and its change due to temperature variation.

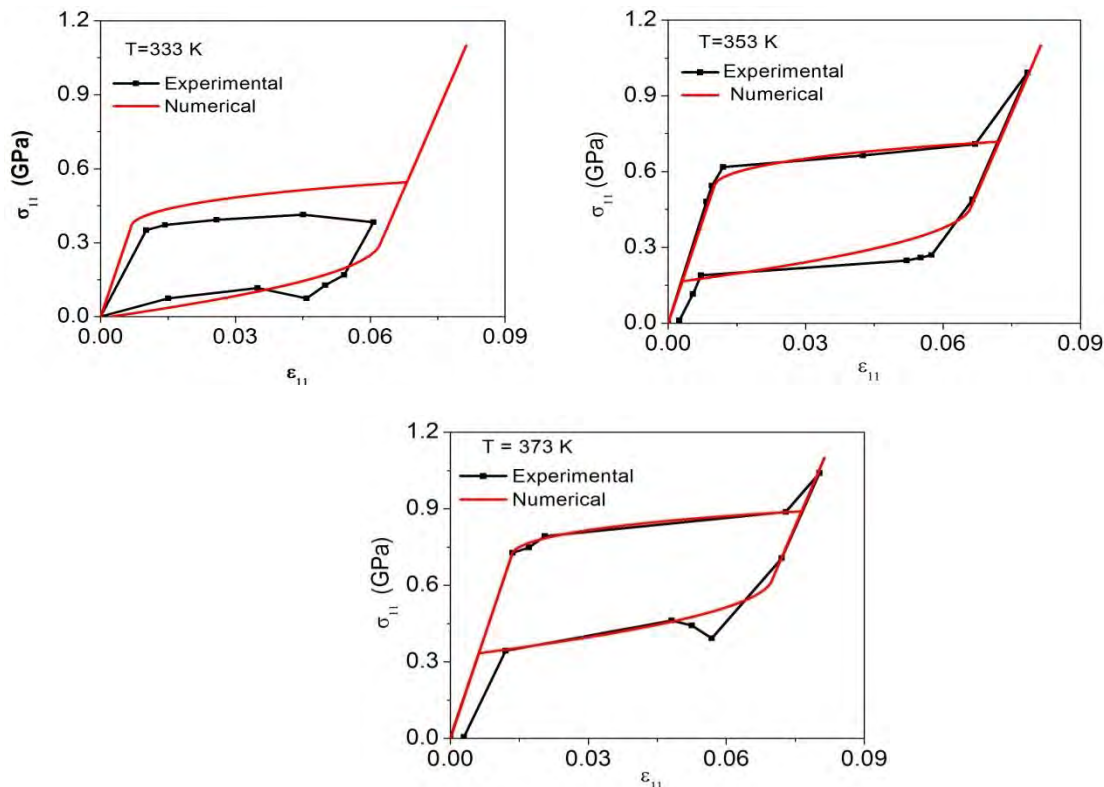


Figure 4 - Numerical-experimental comparison for  $T = 333$  K,  $T = 353$  K and  $T = 373$  K.

Shaw & Kyriakides (1995) observed that the SMA behavior has a rate-dependent behavior. This dependence is a consequence of thermomechanical couplings (Monteiro Jr et al., 2010). Nevertheless, it is possible to represent this behavior as a dissipative behavior. The proposed model is capable to describe this behavior. Figure 5 presents stress-strain curves for different loading rates. Note the rate-dependent response that can be controlled by model parameters.

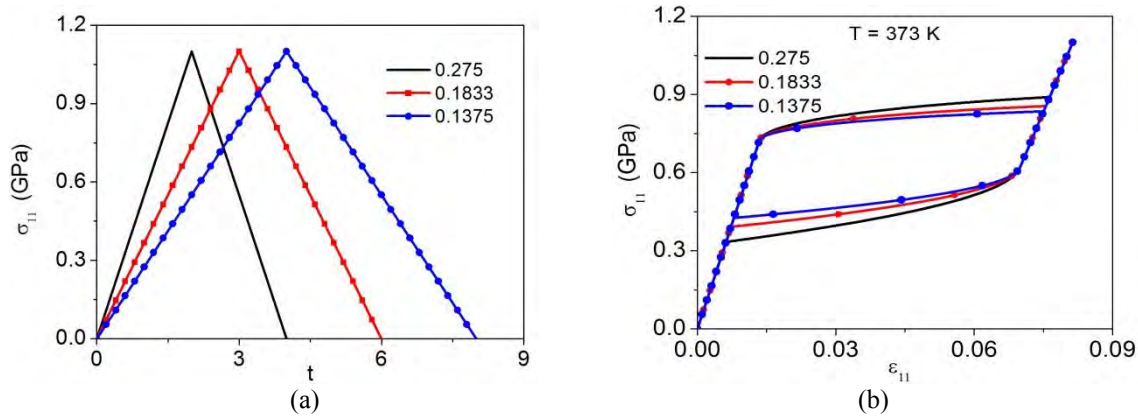


Figure 5 - Loadings with different taxes (a) Loading history in function of the time; (b) Hysteresis curves in function of the loadings rates.

Let us now focus our attention in the shape memory effect. The sample of SMA starts at  $T = 260\text{ K}$ , temperature in which the martensitic is stable in a stress-free state. Afterward, the sample is subjected to a mechanical loading. Initially, mechanical loading causes martensitic reorientation represented by the transformation from the twinned martensite ( $M$ ) to detwinned martensite ( $M^+$ ). After the phase transformation is finished, yield surface is reached during the loading. Afterward, the sample is subjected to a mechanical unloading process, where phase transformation does not take place and, as a consequence, the sample presents a residual strain. After the load-unloading process, the sample is subjected to a thermal loading where temperature increase promotes phase transformation from martensite to austenite. Figures 6a and 6b present the thermomechanical loading-unloading process. Figure. 6c presents the stress-strain-temperature curve showing the whole process while Figure 6d presents the volume fractions evolution. Once again, it should be noticed that the proposed model captures the general thermomechanical behavior for SMAs.

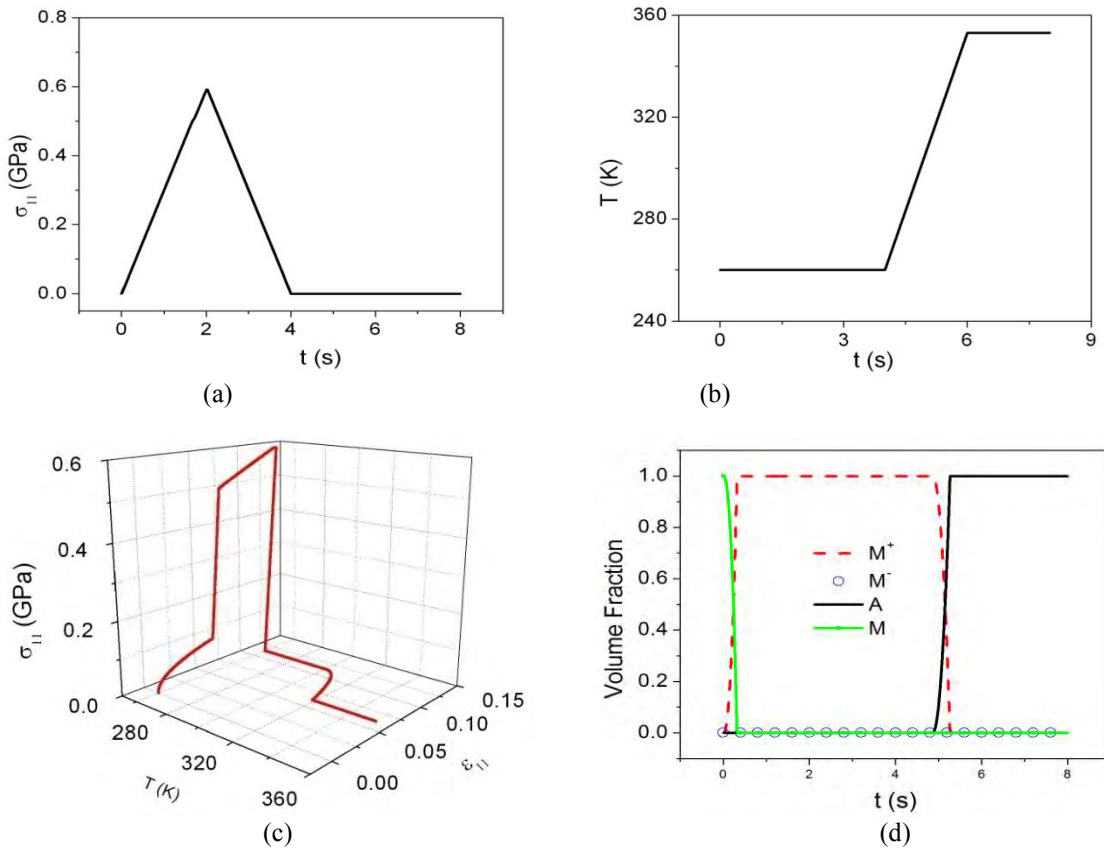


Figure 4.3 – (a) Mechanical loading history; (b) Thermal loading history; (c) Stress-strain-temperature curve; (d) Volume fraction evolution.

A pseudoelastic behavior is now in focus by imposing a cyclic mechanical loading process shown in Figure 7 together with a constant temperature. Under this loading process, incomplete phase transformations are induced, as can be observed in Figure 8, presented as stress-strain curve and time evolution of volume fraction.

Sergio A. Oliveira, Marcelo A.Savi, Nestor Zouain  
 A Three-dimensional Description of Shape Memory Alloy Thermomechanical Behavior Including Plasticity

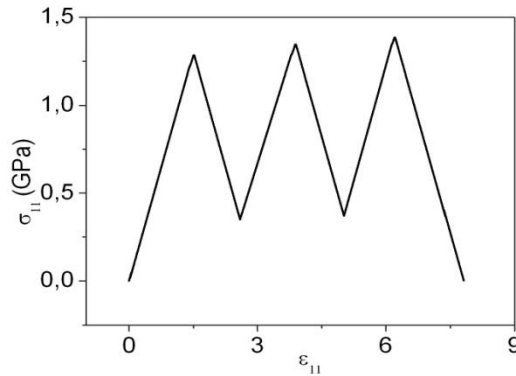


Figure 7 – Cyclic mechanical loading process.

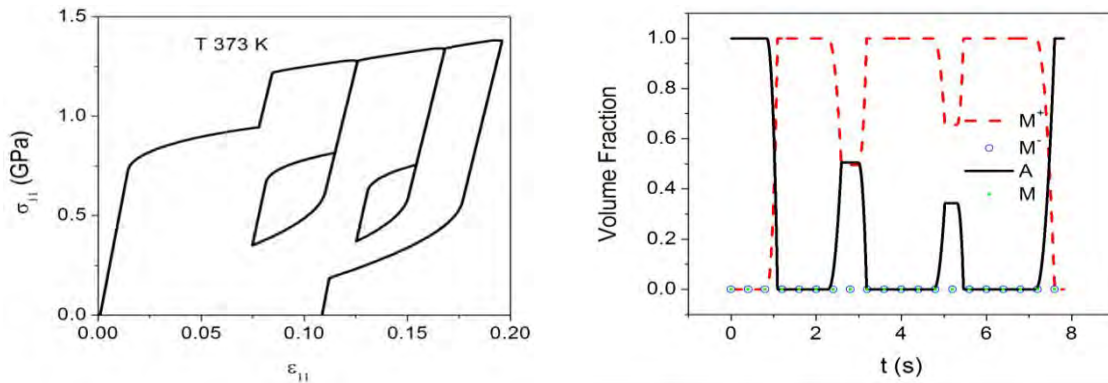


Figure 8 - Pseudoelastic behavior with internal subloops.

The plastic behavior of an SMA sample is now of concern by assuming different loading processes. Initially, a cyclic loading with constant maximum stress of 1.3 GPa is imposed to the sample. Figure 9a shows the loading history while Figure 9b presents the stress-strain curve. Note that the plastic strains tend to stabilize promoting a stabilization of the stress-strain diagram in a specific hysteresis loop.

A different behavior is observed in Figure 10 where loading history has maximum stress values that vary progressively from 1.0 GPa to 1.3 GPa. Figure 10a shows the loading history while Figure 10b presents stress-strain curve. Under this new condition, a different evolution occurs and the plastic strains do not stabilize during the process.

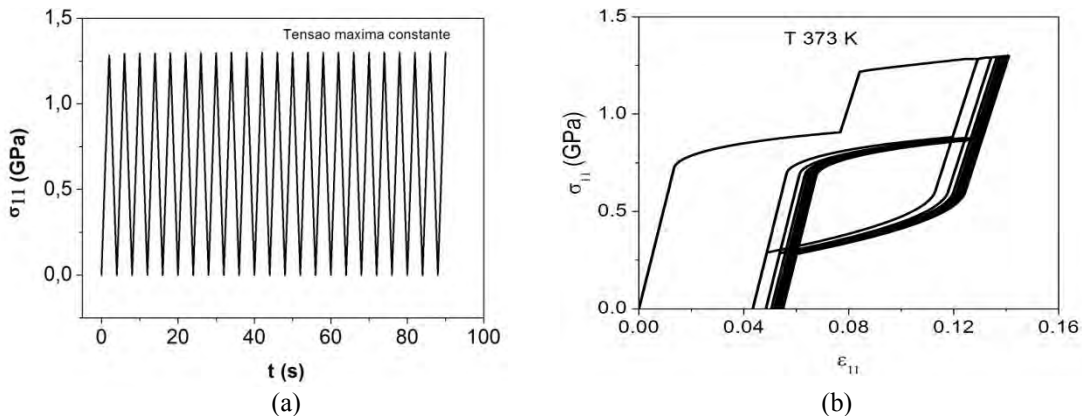


Figure 9 - Pseudoelastic and plastic behaviors. (a) Loading history; (b) Stress-strain curve.

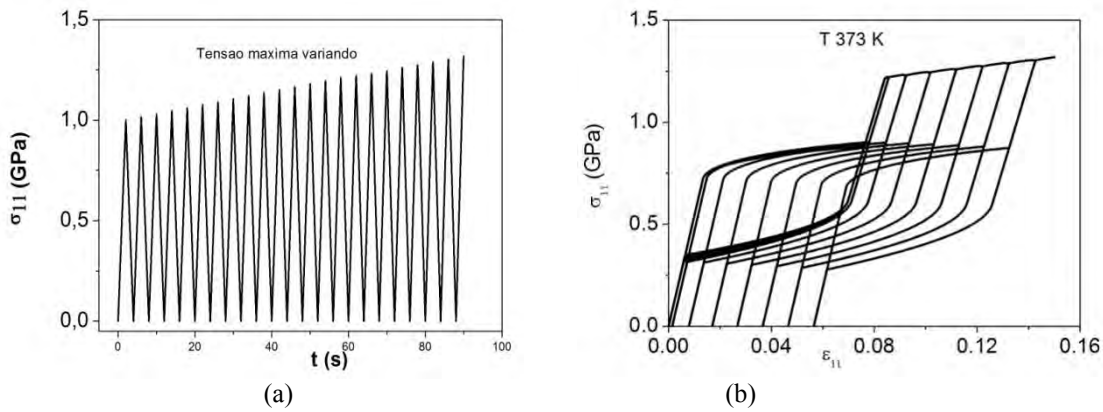


Figure 10 - Pseudoelastic and plastic behaviors.(a) Loading history; (b) Stress-strain curve.

4. NUMERICAL SIMULATIONS – MULTIAXIAL TESTS

This section deals with numerical simulations of multiaxial tests. Initially, pure shear test is of concern, comparing both shear stress loading and the equivalent tension-compression loading. Afterward, a coupled tension-shear test is performed based on the experimental tests by Sittner et al. (1995).

The analysis of a pure shear stress test allows us to verify the coordinate invariance by establishing a comparison between this process with the equivalent tension-compression test. Therefore, two different situations are compared, expressed by the maximum values of the stress tensors that follows:

$$\sigma^C = \begin{bmatrix} 1.1 & 0 & 0 \\ 0 & -1.1 & 0 \\ 0 & 0 & 0 \end{bmatrix} \text{GPa} \quad \sigma^D = \begin{bmatrix} 0 & 1.1 & 0 \\ 1.1 & 0 & 0 \\ 0 & 0 & 0 \end{bmatrix} \text{GPa} \quad (71)$$

Both tests are carried out at temperature  $T = 373 \text{ K}$ . Figure 11 shows the SMA response presenting the stress-strain curves and the volume fractions evolution, comparing the following curves:  $\sigma_{11} \times \epsilon_{11}$  and  $\sigma_{12} \times \epsilon_{12}$ . The response is a typical pseudoelastic behavior and it is important to note that curves are identical, confirming invariance of the system of coordinates.

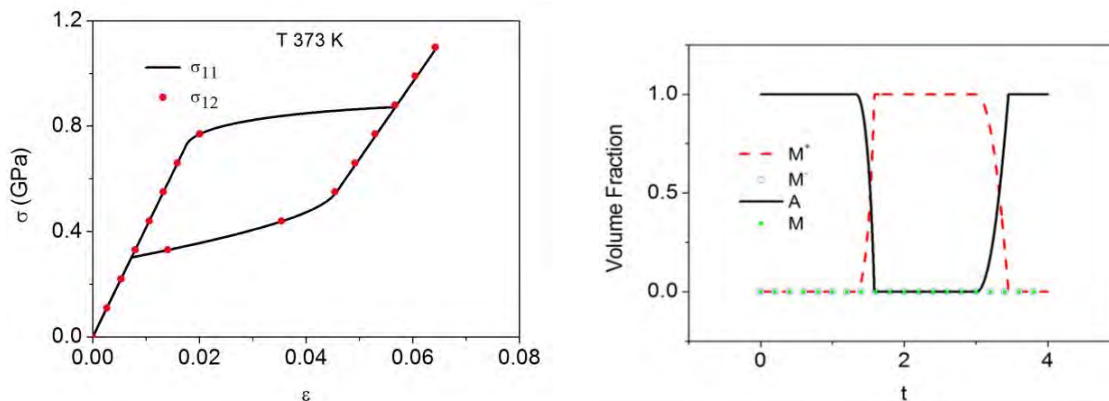


Figure 11 - Comparison between pure shear and equivalent tension-compression tests.

A coupled tension-shear test based on the experimental results of Sittner et al. (1995) is now in focus. Initially, model parameters are adjusted by considering uniaxial tension test and shear tests, separately. Afterward, the coupled test is carried out. Table 2 presents model parameters employed to match uncoupled experimental tests.

Sergio A. Oliveira, Marcelo A.Savi, Nestor Zouain

A Three-dimensional Description of Shape Memory Alloy Thermomechanical Behavior Including Plasticity

Table 2 - Model parameters based on experimental tests due to Sittner et al. (1995).

$E^A$ (GPa)	$E^M$ (GPa)	$\Omega^A$ (MPa/K)	$\Omega^M$ (MPa/K)	$\alpha_N^h$ (MPa)	$\alpha_S^h$ (MPa)	$\alpha$ (MPa)
30	29	0.74	0.17	0.013	0.0108	10
$L_0^+$ (MPa)	$L^+$ (MPa)	$L_0^A$ (MPa)	$L^A$ (MPa)	$T^M$ (K)	$T_0$ (K)	$T^A$ (K)
0.01	7.05	2	35	223	285	260
$T^{A,f}$ (K)	$\sigma_Y^M$ (GPa)	$\sigma_Y^{A,i}$ (GPa)	$\sigma_Y^{A,f}$ (GPa)	$K^A$ (GPa)	$K^M$ (GPa)	$H^A$ (GPa)
423	0.5	1.5	1	1.4	0.4	4
$H^M$ (GPa)	$\eta^l$	$\eta^k$	$\eta_L^+$ (MPa.s)	$\eta_U^-$ (MPa.s)	$\eta_L^-$ (MPa.s)	$\eta_U^-$ (MPa.s)
1.1	-0.01	-0.01	0.1	0.1	0.1	0.1
$\eta_U^A$ (MPa.s)	$\eta_U^M$ (MPa.s)	$\nu^A$	$\nu^M$			
0.1	0.1	0.36	0.36			

Initially, uncoupled tests are presented in Figure 12 showing the comparison between numerical results and experimental data due to Sittner et al. (1995) for tension and shear tests, assuming a loading rate 200MPa/s. Afterward, a tension-shear coupled model is in focus. The SMA sample is subjected to a loading process presented in Figure 13 at a constant temperature. The SMA response is presented in different ways. Stress-strain curves ( $\sigma_{11} \times \varepsilon_{11}$  and  $\sigma_{12} \times 2\varepsilon_{12}$ ) are presented in Figure 14 while Figure 15 presents the strain curve  $\varepsilon_{11} \times 2\varepsilon_{12}$ . It is possible observe that the model captures the general qualitative behavior of the SMA behavior in three-dimensional media with coupled loadings.

In Figure 14 (a) verifies that the tensile loading and unloading presents a linear behavior, without a phase transformation. This linear behavior is found in Fig 14(a) between points A and B and points C and D, for the tensile loading and unloading, respectively.

In Figure 14 (b), the shear loading and unloading exhibit a linear behavior following a non-linear between the points B and C, which is the beginning and the end of shear loading, respectively. Between points C and D shows a linear behavior that is caused by tensile unloading. Between points C and D there is no influence of shear stress, because it is constant. Between points D and E, during the unloading shear is the beginning of nonlinear behavior due to the reverse phase transformation. This nonlinear behavior is shown in Fig at 14(b) in slope part between points B and C and between points D and E, for the shear unloading.

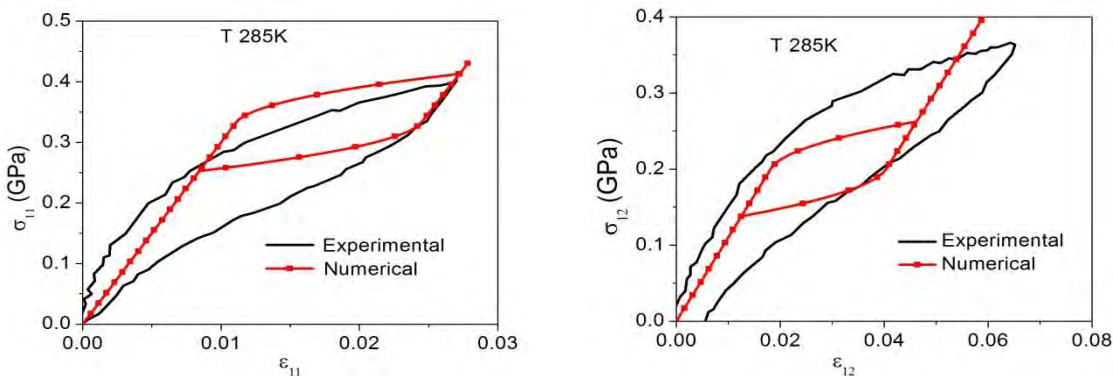


Figure 12 - Tension and shear uncoupled tests.

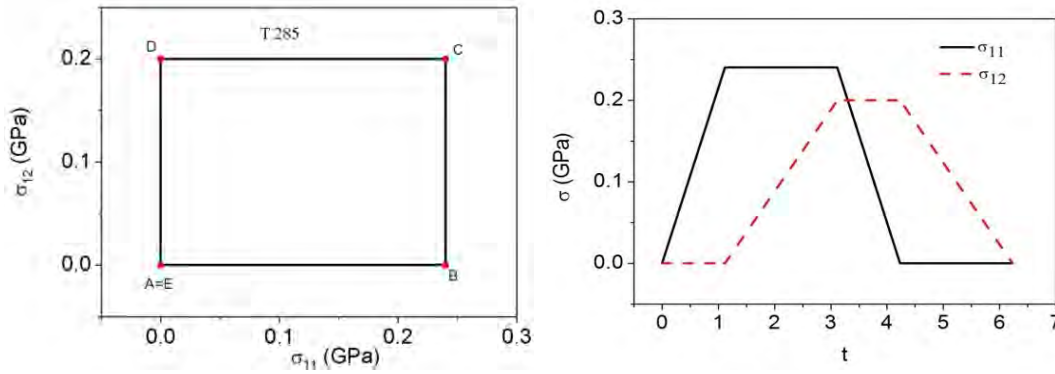


Figure 13 - Loading process of the coupled tension-shear test.

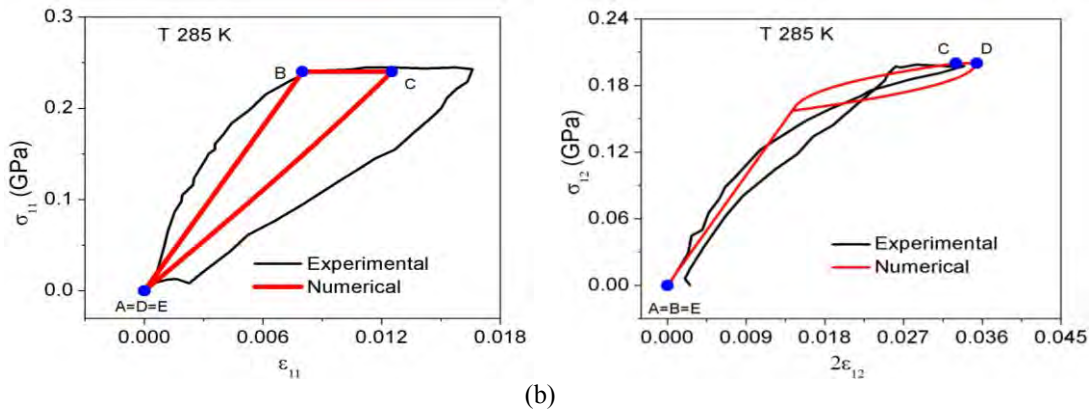


Figure 14 – (a) Tension coupled test, (b) shear coupled test: stress-strain curves.

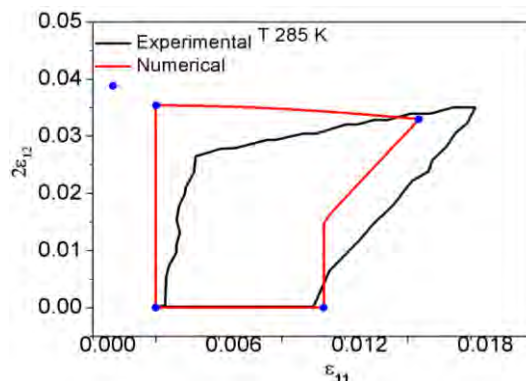


Figure 15 – Tension-shear coupled test: strain curves.

At this point, plastic behavior is of concern assuming the same test previously performed but increasing the stress values in order to reach the yield surface. Figures 16 and 17 show the SMA behavior establishing a comparison with the previous case that does not reach the yield surface. Note that the plastic effect changes the SMA behavior.

Sergio A. Oliveira, Marcelo A.Savi, Nestor Zouain

## A Three-dimensional Description of Shape Memory Alloy Thermomechanical Behavior Including Plasticity

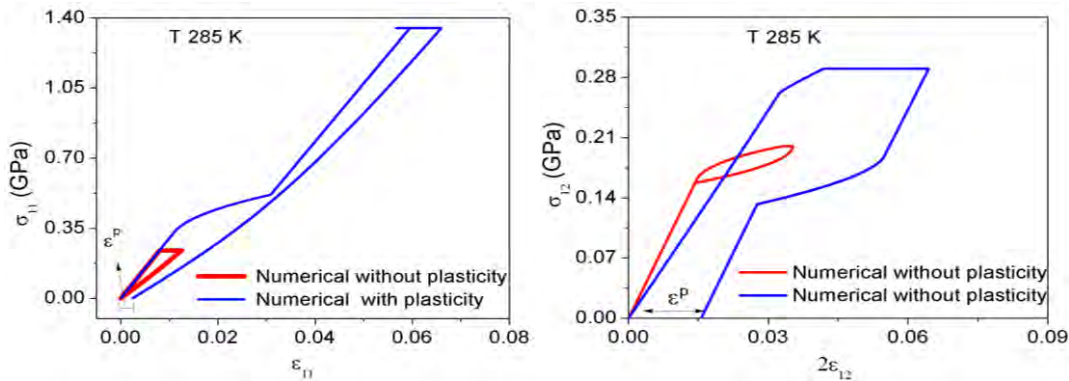


Figure 16 – Tension-shear coupled test: stress-strain curves.

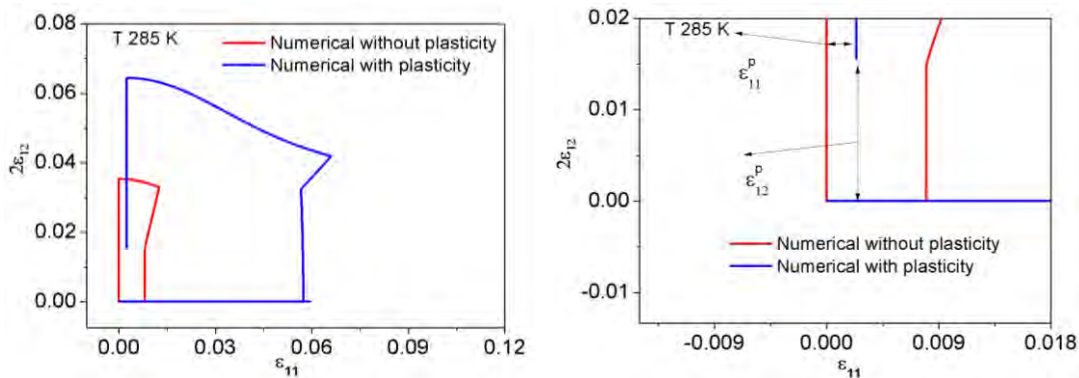


Figure 17 – Tension-shear coupled test: strain curves.

## 5. CONCLUSION

This article presents a three-dimensional macroscopic constitutive model for SMAs. Four macroscopic phases are considered assuming different properties for austenitic and martensitic phases. Plasticity phenomenon is also considered by assuming both kinematic and isotropic hardening effects. An iterative numerical procedure based on the operator split technique is employed. Projection algorithm is employed for phase transformation simulation while return mapping algorithm is employed for plastic simulation. Numerical simulations are treated considering uniaxial and multiaxial tests. The uniaxial tests show the model capability to describe classical phenomena as pseudoelasticity, shape memory effect and internal subloops due to incomplete phase transformation. Moreover, some elastoplastic phenomena are treated. Concerning multiaxial tests, the material invariance is confirmed by establishing a comparison between the pure shear test with the equivalent tension-compression test. Afterward, a coupled tension-shear test is of concern. Model parameters are adjusted by considering tension and shear tests separately and then the model is employed to simulate a shear-tension coupled test. In general, the model is able to capture the general thermomechanical behavior of uniaxial and multiaxial tests. Besides, it should be highlighted the model flexibility since it describes all phenomena using the same set of parameters.

## 6. ACKNOWLEDGEMENTS

The authors would like to acknowledge the support of the Brazilian Research Agencies CNPq, CAPES and FAPERJ and through the INCT-EIE (National Institute of Science and Technology - Smart Structures in Engineering) the CNPq and FAPEMIG. The Air Force Office of Scientific Research (AFOSR) is also acknowledged.

## 7. REFERENCES

- Aguiar, R. A. A.; Savi, M. A.; Pacheco, P. M. C. L., “Experimental and Numerical Investigations of Shape Memory Alloy Helical Springs”, *Smart Materials & Structures*, v.19, n.2, Article Number: 025008, 2010.
- Auricchio, F.; Reali, A.; Stefanelli, U., 2007, “A Three-Dimensional Model Describing Stress-Induced Solid Phase Transformation with Permanent Inelasticity”, *International Journal of Plasticity*, v.23, pp.207–226, 2007.
- Baêta-Neves, A. P.; Savi, M. A.; Pacheco, P. M. C. L., “On the Fremond’s Constitutive Model for Shape Memory Alloys”, *Mechanics Research Communication*, v.31, pp. 677-688, 2004.

- Brocca, M.; Brinson, L.C. & Bazant, Z.P., "Three-Dimensional Constitutive Model for Shape Memory Alloys Based on Microplane Model", *Journal of the Mechanics and Physics of Solids*, v.50, pp.1051–1077, 2002.
- Fremond, M., "Shape Memory Alloy: A Thermomechanical Macroscopic Theory", *CISM Courses and Lectures*, n.351, pp.3-68, New York, 1996.
- Jackson C.M; Wagner, H. J.; Wasilewski, R. J., "55-Nitinol –The Alloy with a Memory: Its Physical Metallurgy, Properties, and Applications, Nasa-SP -5110, 1972.
- Grabe, C.; Bruhns, O. T., "Tension-Torsion Tests of Pseudoelastic, Polycrystalline NiTi Shape Memory Alloys under Temperature Control", *Material Science Engineering A - Structural Materials Properties Microstructure and Processing*, v.481, pp. 109-113, 2008.
- Hartl, D. J.; Chatzigeorgiou, G.; Lagoudas, D. C., "Three-Dimensional Modeling and Numerical Analysis of Rate-Dependent Irrecoverable Deformation in Shape Memory Alloys", *International Journal of Plasticity*, v. 26, n.10, pp. 1485-1507, 2010.
- Kalamkarov, A. L.; Kolpakov, A. G., "Analysis, Design and Optimization of Composite Structures", John Wiley & Sons, New-York, 1997.
- Lagoudas, D. C., "Shape Memory Alloys: Modeling and Engineering Applications", Springer, 2008.
- Lemaitre, J.; Charboche, J. L., "Mechanics of Solid Materials", Cambridge University Press, 1990.
- Levitas, V. I.; Preston, D. L.; Lee, D.-W., "Three-dimensional Landau Theory for Multivariant Stress-induced Martensitic Phase Transformations. III. Alternative Potentials, Critical Nuclei, kink Solutions, and Dislocation Theory", *Physical Review B*, v.68, 134201, 2003.
- Machado, L. G.; Savi. M. A., "Medical Applications of Shape Memory Alloys", *Brazilian Journal of Medical and Biological Research*, v.36, n. 6, pp.302-306, 2003.
- Manach, P.; Favier, D., "Shear and Tensile Thermomechanical Behavior of Near Equiatomic NiTi Alloy", *Material Science and Engineering A222*, pp.45-47, 1997.
- McNaney, J.M.; Imbeni, V.; Jung, Y.; Papadopoulos, P.; Ritchie, R.O. "An Experimental Study of the Superelastic Effect in a Shape-Memory Nitinol Alloy under Biaxial Loading", *Mechanics of Materials*, v.35, pp.969-986, 2007.
- Oliveira S. A.; Savi M. A., Kalamkarov, A. L. "A Three-Dimensional Constitutive Model For Shape Memory Alloys", *Archive of Applied Mechanics*, v. 80, Issue: 10, pp. 1163-1175, 2010.
- Ortiz, M.; Pinsky; P.M.; Taylor, R.L., *Operator Split Methods for The Numerical Solution of The Elastoplastic Dynamic Problem*, *Computer Methods of Applied Mechanics and Engineering*, 39, pp.137-157, 1983.
- Paiva, A.; Savi, M. A. "An Overview of Constitutive Models for Shape Memory Alloys", *Mathematical Problems in Engineering*, Article ID56876, Vol. 2006, pp. 1-30, 2006.
- Paiva A.; Savi M.A.; Braga, A.M.B & P.M.C.L. Pacheco, "A Constitutive Model for Shape Memory Alloys Considering Tensile-Compressive Asymmetry and Plasticity", *International Journal of Solids and Structures*, Vol.42, no 11-12, pp.3439-3457, 2005.
- Panico, M.; Brinson, L. C., "A Three-Dimensional Phenomenological Model for Martensite Reorientation in Shape Memory Alloy", *Journal of the Mechanics and Physics of Solids*, doi:10.1016/j.jmps.2007.03.010, 2007.
- Popov, P.; Lagoudas, D. C., "A 3-D Constitutive Model for Shape Memory Alloys Incorporating Pseudoelasticity and Detwinning of Self-accommodated Martensite", *International Journal of Plasticity*, 23, pp.1679–1720, 2007.
- Rockafellar, R. T., "Convex Analysis", Princeton Press, New Jersey, 1970.
- Savi, M. A., Braga, A.M.B., "Chaotic Vibration of Oscillator with Shape Memory" *Journal of The Brazilian Society for Mechanical Sciences* 15 (1), pp.1-20, 1993.
- Savi, M.A.; Paiva, A., Describing Internal Subloops Due to Incomplete Phase Transformations in Shape Memory Alloys, *Archive of Applied Mechanics*, 74 (9), pp.637-647, 2005.
- Savi, M. A.; Paiva A.; Baeta-Neves A. P.; Pacheco P. M. C. L., "Phenomenological Modeling and Numerical Simulation of Shape memory: A Thermo-Plastic-Phase Transformation Coupled Model", *Journal of Intelligent Materials Systems and Structures*, 3 (5), pp. 261-273, 2002.
- Schroeder, T.A.; Wayman, C.M., *The Formation of Martensite and The Mechanism Of The Shape Memory Effect in Single Crystals Of Cu-Zn Alloys*, *ACTA Metallurgica*, 25, pp.1375, 1977.
- Shaw, J. A.; Kyriades, S., "Thermomechanical Aspects of Ni-Ti", *Journal of the Mechanics and Physics of Solids*, 43 (8), pp.1243-1281, 1995.
- Simo, J. C. & Hughes, T. J. R. , "Computational Inelasticity", Springer, 1998.
- Sittner, P., Hara, Y. and Tokuda, M. " Experimental Study on the Thermoelastic Martensitic Transformation in Shape Memory Alloy Polycrystal Induced by Combined External Forces, *Metall. Mater. Trans.*, Vol. 26a, pp. 2923-2935, 1995.
- Souza, A.C.; Mamiya, E. N.; Zouain, N. "Three-Dimensional Model for Solids Undergoing Stress-nduced Phase Transformations". *European Journal of Mechanics - A Solids*, 17: pp. 189-806, 1998.
- Tobushi, H, et al "Deformation Behavior of Ni-Ti Shape Memory Alloy Subjected to Variable Stress and Temperature", *Continuum Mechanics Thermodynamics*, Vol. 3, pp. 79-93, 1991.
- Wang, Y. F.; Yue, Z. F.; Wang, J. "Experimental and Numerical Study of the Supereslastic Behavior on NiTi Thin-

Sergio A. Oliveira, Marcelo A.Savi, Nestor Zouain

A Three-dimensional Description of Shape Memory Alloy Thermomechanical Behavior Including Plasticity

walled Tube under Biaxial Loading”. Computational Materials Science Vol.40, no. 2, pp. 246-254, 2007.

Zaki, W.; Moumni, Z., “A three-dimensional Model of the Thermomechanical Behavior of Shape Memory Alloys”, Journal of the Mechanics and Physics of Solids, doi:10.1016/j.jmps.2007.03.012, 2007.

Zhang, X.D.; Rogers, C.A.; Liang ,C., “Modeling of Two-way Shape Memory Effect”, Smart Structures and Material - ASME, pp. 79-90, 1991.

#### **8. RESPONSIBILITY NOTICE**

The author(s) is (are) the only responsible for the printed material included in this paper.